Int. J. Electrochem. Sci., 10 **(2015)** 1343 - 1360

International Journal of
ELECTROCHEMICAL
SCIENCE
www.electrochemsci.org

Corrosion Inhibition of X-65 Carbon Steel in Oil Wells Produced Water under CO_2 Environment

M. A. Migahed[1], *M. M. Attya*[2], *M. Abd El-raouf*[1,*], *E. A. Khamis*[1], *T. A. Ali*[1] *and A. M. Al-Sabagh*[1]

[1] Egyptian Petroleum Research Institute, Nasr city, Cairo (11727), Egypt
[2] Production Engineering Department, Badr Petroleum Company (BAPETCO), Heliopolis, Cairo, Egypt
[*]E-mail: abdelraouf1979@yahoo.com

Received: 27 October 2014 / *Accepted:* 8 December 2014 / *Published:* 16 December 2014

Corrosion behavior of X-65 type carbon steel exposed to CO_2 saturated oil well produced water was studied in the absence and presence of new synthesized; ethoxy- (5-methyl-benzotriazol-1-yl) (EMB) at 50 ^oC by both potentiodynamic polarization and electrochemical impedance (EIS) techniques. Results indicated that the inhibitor retards both cathodic and anodic reactions and acts as mixed type inhibitor. SEM technique confirmed formation of a good protective film on metal surface which imparts the high inhibition efficiency. The results were discussed in the light of quantum chemical calculations to provide theoretical interpretation of the inhibitor performance.

Keywords: Carbon steel; Ethoxy-2(5-methyl-benzotriazol-1-yl) ; EIS; Polarization; SEM; Acid corrosion; Acid inhibition.

1. INTRODUCTION

Carbon steels are the most commonly used material of construction for petroleum production assets. Carbon steels are susceptible to severe corrosion in process environments containing carbon dioxide [1]. Natural gas is most likely contains carbon dioxide as part from reservoir fluid composition, on other hand CO_2 can be injected for enhanced oil recovery purposes. As such, corrosion control in carbon dioxide containing media is area of concern for oil field industries [2,3]. Process operating parameters, especially temperature, pressure and fluid composition, are generally contributing to corrosion behavior for such conditions [4]. Extensive investigation studies had been

carried out to understand and control CO_2 corrosion [5]. CO_2 dissolves in oil wells produced water forming carbonic acid which in turn dissociates and decrease the solution pH:

$$CO_{2(g)} + H_2O_{(l)} = H_2CO_{3(aq.)} \quad (1)$$

$$H_2CO_{3\,(aq.)} = H^+ + HCO_3^- \quad (2)$$

$$HCO_3^- = H^+ + CO_3^{2-} \quad (3)$$

In view of the above mentioned conditions, CO_2 corrosion had been proposed as follows:

Firstly, the cathodic reaction can proceed by one of the following reactions:

$$2H_2CO_3 + 2e^- = H_2 + 2HCO_3^- \quad (4)$$

$$2HCO_3^- + 2e^- = H_2 + 2CO_3^{2-} \quad (5)$$

$$2H^+ + 2e^- = H_2 \quad (6)$$

Secondly, the anodic reaction can take place through:

$$Fe = Fe^{2+} + 2e^- \quad (7)$$

Under such conditions, a ferrous carbonate corrosion scale can be formed according to :

$$Fe^{2+} + CO_3^{2-} = FeCO_3 \quad (8)$$

The nature of oxide/passive film resulted from a corrosion process contributes to the overall behavior of it as well as temperature and chemical composition of the aqueous media [6,7]. Surfactants are most likely corrosion inhibitors employed in the petroleum industry to protect iron and steel equipment used in drilling, production, transport and refining of hydrocarbons [8,9]. The efficiency of the applied corrosion inhibitor depends on its concentration and stability of the formed inhibition film on metal surface. Ethylene oxide units are introduced to surfactant molecule in order to increase the inhibitive effect of surfactant [10]. The presence of these groups increases the solubility of surfactant and hence the extent of its adsorption on the metal surface and consequently its inhibitive action improves. Intensive studies had been carried out to evaluate the inhibition efficiency of ethoxylated surfactants in a lot of corrosive environments [11-16]. The present study is aimed to assess the performance of a new synthesized EMB poly ethoxylated nonionic surfactant as corrosion inhibitor for X-65 carbon steel in oil wells produced water under CO_2 environment at 50 ^oC.

2. EXPERIMENTAL

2.1. Chemical composition of the investigated carbon steel alloy

Table 1. Chemical composition of carbon steel alloy

Element	C	Si	Mn	P	S	Ni	Cr	Mo	V	Cu	Al	Fe
Content (Wt %)	0.09	0.22	1.52	0.01	0.05	0.04	0.02	0.004	0.002	0.02	0.04	rest

Table (1) shows the chemical composition of carbon steel samples used in this investigation which is selected to resemble the most likely used alloy in oil and gas transportation pipelines.

2.2. Oil well produced water

Produced water is normally produced in line with oil and gas production as being part from reservoir aquifer formation. It usually may contain sodium, calcium, magnesium, chloride, bicarbonate and sulfate. Table (2) shows the chemical composition of oil well produced water used in this investigation.

Table 2. Chemical composition and physical properties of deep oil well produced water used in this investigation

Physical Properties		
Property	Unit	Value
Density	g/cm^3	1.044
Turbidity	FAU	263
PH		6.38
Salinity as NaCl	mg/l	12029
Conductivity	µS/cm	29220
Total hardness	mg/l	2910
Chemical Properties		
Ionic species	Value	
Sulphate	6.5 (mg/l)	
Phosphate	0.771(mg/l)	
Carbonate	nil	
Bi-carbonate	143 (mg/l)	
Chloride	7300 (mg/l)	
Sulfide	450 (µg/l)	
Iron ferrous	23 (mg/l)	
Iron , Total	42 (mg/l)	
Calcium	800 (mg/l)	
Magnesium	364 (mg/l)	
Barium	105 (mg/l)	
Potassium	250 (mg/l)	
Zinc	1.359 (mg/l)	
T.D.S	15520 (mg/l)	

2.3. Synthesis of the inhibitor

In conventional synthesis flask attached with condenser, magnetic stirrer, thermometer, ethylene oxide gas was allowed to pass over tolyltriazole melt under a controlled pressure of 86-88 cm Hg with stirring at 80-90 ^oC [17-20].

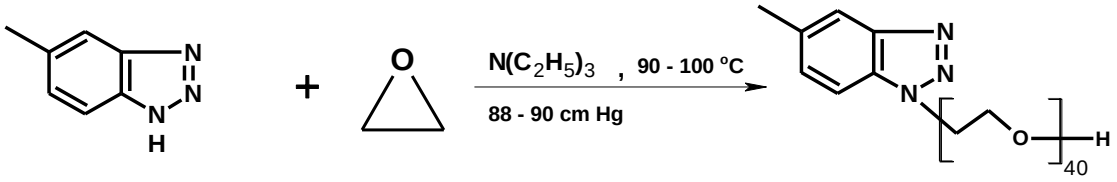

Synthesis of nonionic surfactant

The reaction mixture was refluxed for about 3hrs then after it was cooled and flashed off every 0.5hr to evaluate the gained weight due to ethylene oxide units insertion and hence follow-up the reaction progress. The desired reaction product reached when the weight gained was equivalent to 40 ethylene oxide units.

2.4. Confirmation of the Synthesized Compound

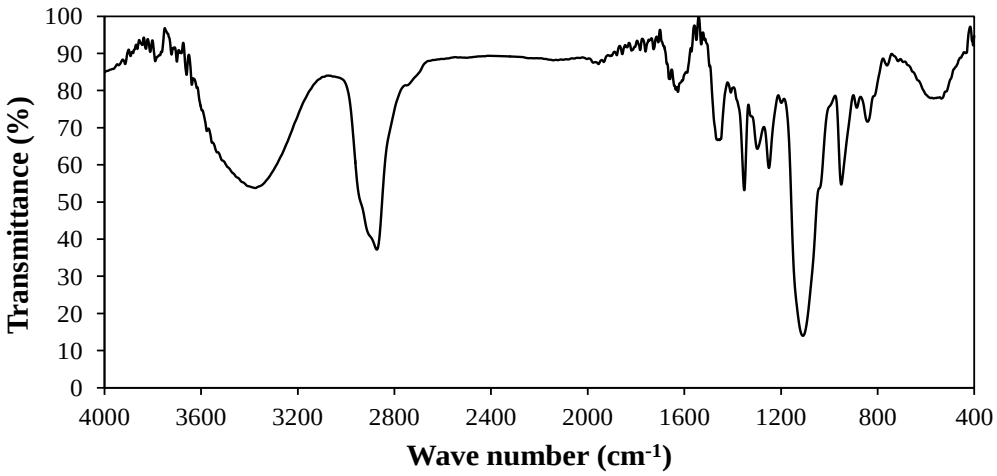

Figure 1. FT-IR spectrum of the Synthesized EMB Inhibitor

Fig. 1 shows IR spectrum of the synthesized nonionic surfactant as recorded using ATI Mattson-Genesis Series FTIRTM infrared spectroscopy. OH stretching vibrations are indicated by strong broad band in the region of 3200–3600 cm^{-1} while C–O ether stretching vibrations indicated by strong band at 1120 cm^{-1}. The incorporation of aliphatic moiety indicated by appearance bands at 2880 cm^{-1} characteristic for aliphatic C–H bonds while C–N stretching vibration confirmed by weak band at 1340 cm^{-1}.

Fig. 2 shows ^{1}H-NMR spectra of the synthesized surfactant as recorded on a DPX300 spectrophotometer (300 MHz) where, ^{1}H-NMR (DMSO) (б, PPM) ,3.49-3.96 (8 CH_2-ALPHA N*R) , 4.1-4.77 (8 CH_2- ALPHA O), 7.1-7.8 (3H, Ar-H) , 2.44-2.74 (3H,CH_3).

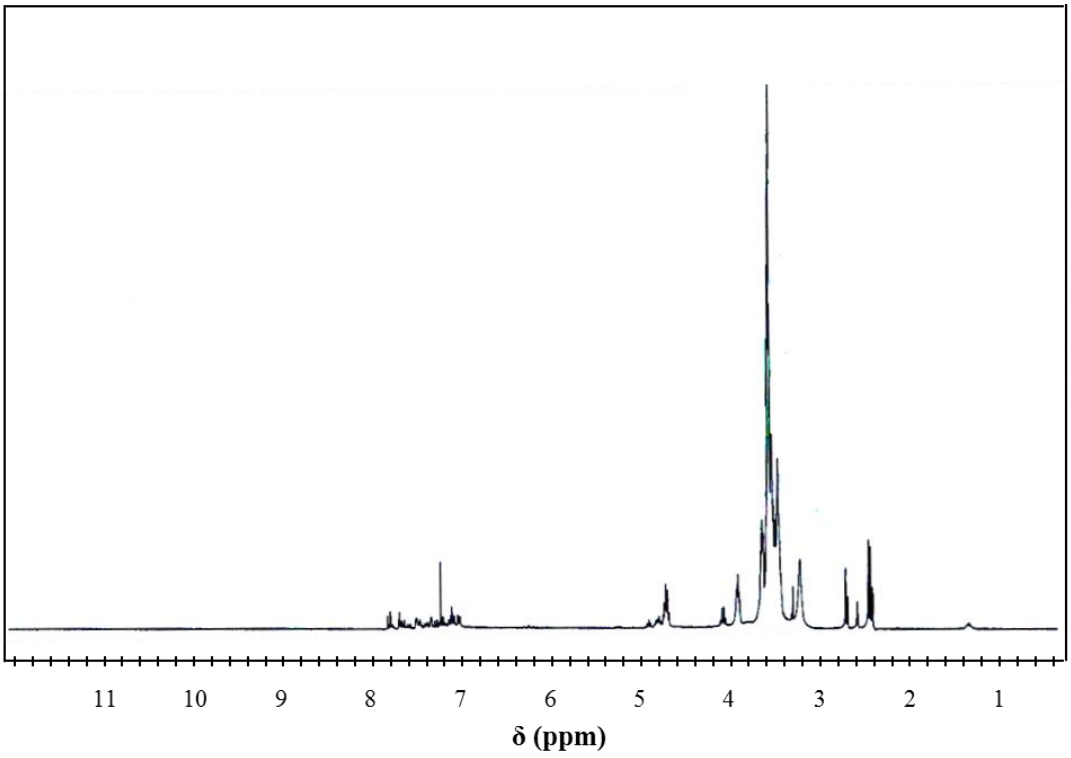

Figure 2. ^{1}H NMR spectrum of the synthesized inhibitor

2.5. Potentiodynamic polarization measurements

The experiments were carried out in CO_2 saturated produced water at 50 ^{o}C. Platinum electrode was used as counter electrode and calomel as reference electrode. Volta lab80 (Tacussel-radiometer PGZ402) potentiostat was used for electrochemical polarization measurements which controlled by Tacussel corrosion analysis software model (Volta master 4). In this method the working electrode was immersed in the test solution for 2 hours until the open circuit potential is established. After that the working electrode was polarized in both cathodic and anodic directions. All potentials were measured against a saturated calomel electrode (SCE) as a reference electrode, where as a platinum electrode was used as an auxiliary electrode. The polarization curves were recorded by change the electrode potential automatically from -1200 mV to -400 mV with a scan rate 2 mVs^{-1}.

2.6. Electrochemical impedance spectroscopy (EIS)

Nyquist and Bode plots for various concentrations of the investigated inhibitor were carried out using Volta lab 80 potentiostat (Tacussel-radiometer PGZ402) controlled by Tacussel corrosion analysis software model (Volta master 4). The working electrode was immersed in the corrosive media for 3 hrs then impedance measurements were carried out by applying a frequency range of 100 kHz and 50 mHz using 20 steps per frequency decade while 20 mV amplitude peak to peak AC signal was used to perturb the system.

2.7. Surface tension measurements

The surface tension (γ) for various concentrations of the investigated surfactant was measured using Krüss K6 Tensiometer type.

2.8 Scanning electron microscopy

All the specimens of X-65 type steel were degreased by acetone, then abraded by emery papers of grade number 360, 400, 600, 800, 1200 and 2000; finally washed by distilled water and dried. Carbon steel specimen surface was examined using scanning electron microscope (JEOL JSM-5410, Japan) at 20 kV acceleration beam energy. A magnification power of 750 was applied to the resulted micrographs.

2.9. Quantum chemical study

Quantum molecular parameters were calculated according to MINDO3 semi-empirical method used for organic inhibitor's calculation [21] at Unrestricted Hartree Fock (UHF) level which are implemented in Hyperchem 8.0. The molecules 2D sketch was obtained by ISIS Draw 2.1.4.

3. RESULTS AND DISCUSSION

3.1. Potentiodynamic polarization measurements

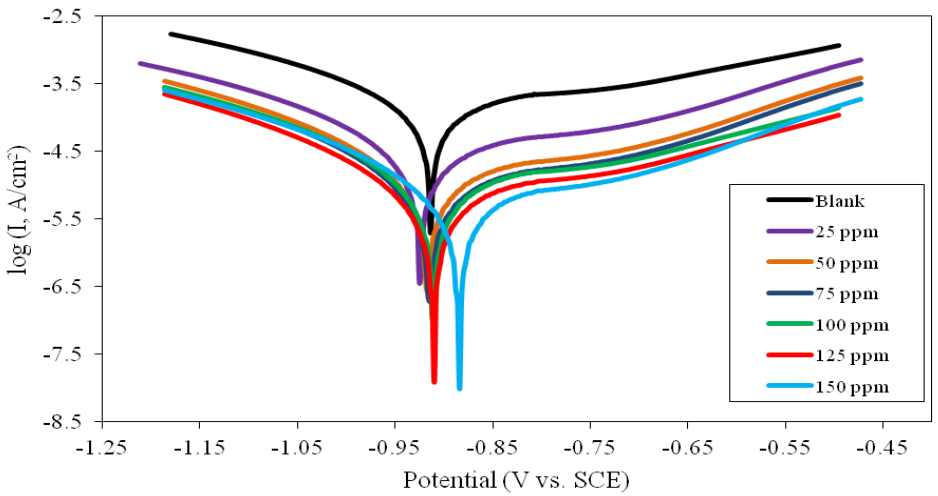

Figure 3. Potentiodynamic polarization curves of carbon steel in produced water in the absence and presence of different concentrations of the inhibitor at 50 ^{o}C

Carbon steel specimen was prepared for electrochemical testing as working electrode and immersed in CO_2 saturated oil well produced water at 50 ^{o}C. Anodic and cathodic polarization curves

were plotted in the absence and presence of various concentrations of the synthesized EMB inhibitor as shown in Fig. 3. Values of corrosion current density ($i_{corr.}$) were calculated from the extrapolation of Tafel lines to pre-determined open circuit potential. The obtained polarization curves indicated that corrosion current density ($i_{corr.}$) was decreased by increasing inhibitor concentration with respect to the inhibitor free solution and hence, formation of good protective layer on the surface of carbon steel.

The following equations were used to calculate degree of surface coverage (θ) and the percentage inhibition efficiency (IE %) [22] :

$$\theta = 1 - i/i_0 \quad (9)$$

$$IE\% = \left(1 - i/i_0\right) \times 100 \quad (10)$$

where i_o and i are the corrosion current densities in the absence and presence of the inhibitor, respectively.

The obtained electrochemical parameters including corrosion potential ($E_{corr.}$), corrosion current density ($i_{corr.}$), cathodic and anodic Tafel slopes (b_c and b_a) and polarization resistance (R_p) were calculated from polarization measurements and summarized in Table (3).

Table 3. Data obtained from potentiodynamic polarization measurements of carbon steel in produced water solution in the absence and presence of various concentrations of the inhibitor at 50 ^{o}C

Conc. (ppm)	$-E_{corr}$ (mV vs. SCE)	I_{corr} (μA/cm²)	R_p (k ohm.cm^2)	β_a (mV dec^{-1})	$-\beta_c$ (mV dec^{-1})	IE (%)
Blank	1031.2	51.106	0.387	97.8	127.6	-
25	1001.5	17.783	1.113	89.1	123.2	65.2
50	1028.1	10.253	1.935	88.3	121.3	79.9
75	1031.9	7.079	2.774	87.5	118.4	86.1
100	1027.7	5.623	3.538	86.2	118.8	89.0
125	1034.2	3.981	4.982	86.9	117.6	92.2
150	1041.7	3.162	6.342	87.8	115.2	93.8

It shows that Tafel lines are shifted to more negative and more positive potentials for the anodic and cathodic processes, respectively relative to the blank curve. This means that the synthesized EMB compound retards both anodic and cathodic reactions, hence it acts as mixed type inhibitor. Also Tafel plots indicated that the synthesized inhibitor has no effect on metal dissolution mechanism since the slopes of the cathodic and anodic Tafel lines are approximately constant and independent on the inhibitor concentration.

3.2. Electrochemical impedance spectroscopy (EIS)

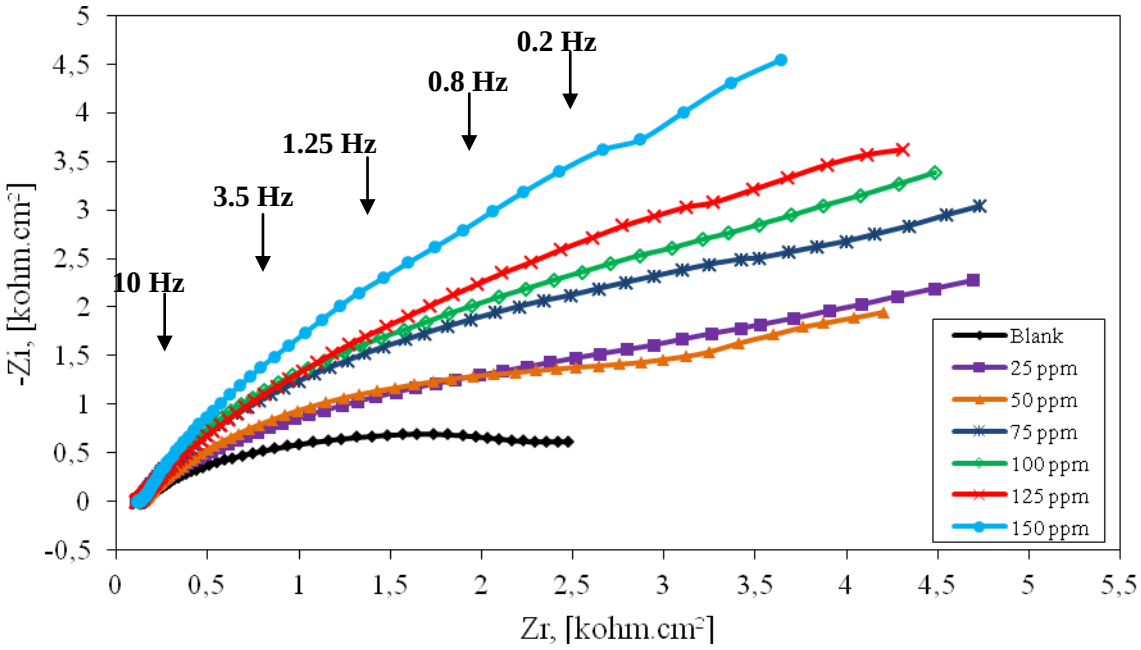

Figure 4. Nyquist plots for carbon steel in oil wells produced water in the absence and presence of different concentrations of the inhibitor at 50 °C

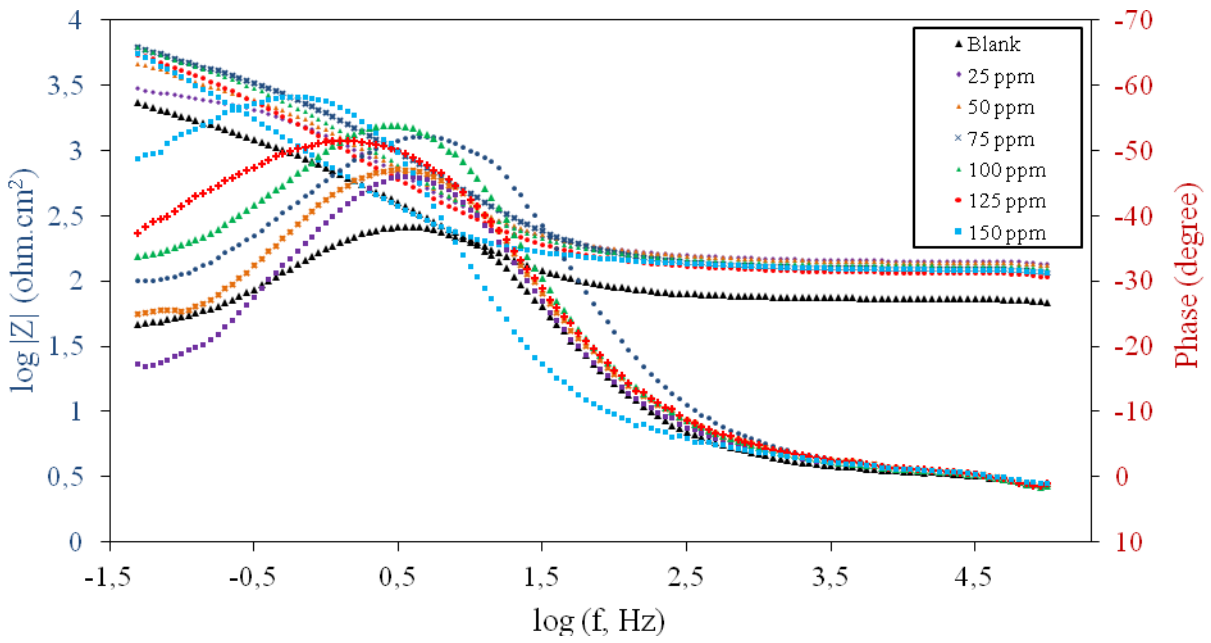

Figure 5. Bode plots for the carbon steel in the oil wells produced water in absence and presence of various concentrations of the inhibitor at 50 °C

Corrosion behavior of carbon steel specimen in CO_2 saturated oil well produced water at 50 °C in the absence and presence of various concentrations of the synthesized inhibitor was investigated by EIS technique. Figs. 4,5 show the obtained Nyquist and Bode plots which indicate that the impedance

response of carbon steel in produced water was significantly changed after the addition of the inhibitor molecules. For analysis of the obtained impedance spectra, the equivalent circuit (EC) was obtained using Boukamp equivalent circuit program as shown in Fig. 6 where R_s is the solution resistance, R_t is the charge transfer resistance, C_{dl} is the electrochemical double layer capacitance, R_f is the film resistance and C_f is the film capacitance.

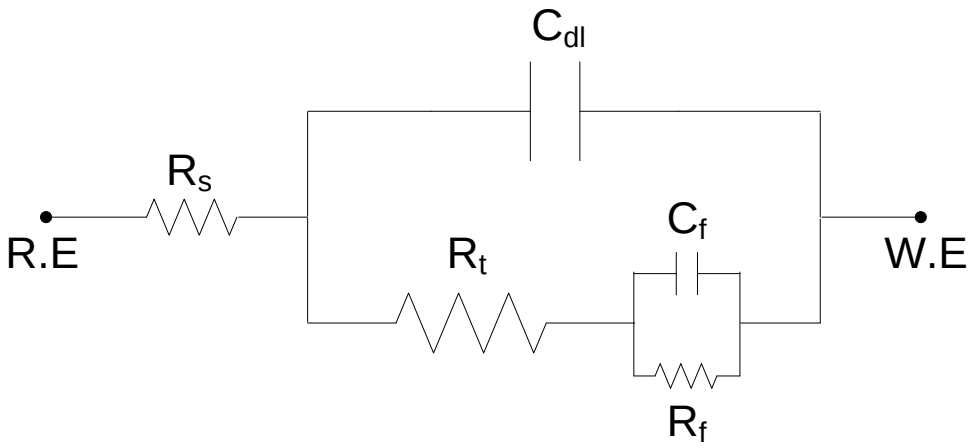

Figure 6. Equivalent ciruit used to model impedance data of carbon steel in produced water saturated with CO_2 in the absence and presence of various concentrations of EMB at 50 ^oC

Table 4. Data obtained from electrochemical impedance spectroscopy (EIS) measurements of carbon steel in produced water solution in the absence and presence of various concentrations of the inhibitor at 50 ^oC

Concentration, (ppm)	Coefficient	R_f, (kohm.cm²)	C_f, (μF/cm²)	R_s, (ohm.cm²)	R_t, (kohm.cm²)	C_{dl}, (μF/cm²)	IE%
Blank	0.979	-	-	131.9	3.0	384.7	-
25	0.999	0.388	62.72	123.1	7.8	295.9	61.5
50	0.999	0.125	50.34	109.2	13.7	276.6	78.1
75	0.972	0.148	43.86	127.9	17.4	266.4	82.8
100	0.994	0.186	38.12	100.7	20.8	251.3	85.6
125	0.991	0.192	27.56	114.9	25.8	231.8	88.4
150	0.988	0.225	22.05	103.1	29.6	176.9	89.7

Table (4) summarized the obtained EIS parameters and the calculated percentage inhibition efficiency IE % according to the following equations.

Charge transfer resistance R_t was calculated from high and low frequency impedance data as follows [23]:

$$R_t = Z'_{re.}(\text{at low frequency}) - Z'_{re.}(\text{at high frequency}) \qquad (11)$$

Electrochemical double layer capacitance C_{dl} was obtained at the frequency f_{max}, at which the imaginary component of the impedance is maximal – Z_{max} using the following equation:

$$C_{dl} = \frac{1}{2\pi f_{max.}} \frac{1}{R_t} \quad (12)$$

Finally, the percentage inhibition efficiency IE % was calculated from the values of R_t using the following equation:

$$IE\% = \left(1 - \frac{R_t}{R_{t(inh)}}\right) \times 100 \quad (13)$$

where R_t and $R_{t\ (inh)}$ are the charge transfer resistance values in the absence and presence of inhibitor, respectively. The applied EMB surfactant inhibited the corrosion rate as indicated by increasing the value of charge transfer resistance ($R_{t)}$ and decreasing the value of double layer capacitance (C_{dl}) with increasing EMB inhibitor concentration, hence inhibiting the corrosion rate on carbon steel surface by adsorption mechanism [24,25]. It was found that the values of film resistance (R_f) were increased by increasing the EMB concentration, while (C_f) values were decreased. This data conform the formation of a good protective film of EMB on carbon steel surface.

3.3. Surface tension measurements

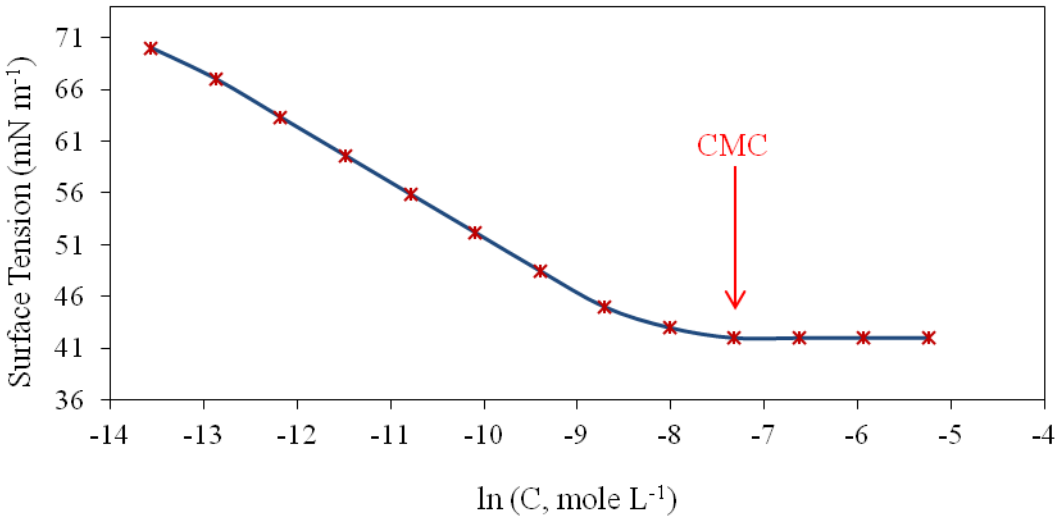

Figure 7. Surface tension (γ) vs. logC at different concentrations of the inhibitor at 50 ^{o}C

Surface tension measurements were carried out for different concentrations of the synthesized EMB inhibitor at 50 ^{o}C. Then values of critical micelle concentration, CMC, was determined from the change in slope of the plotted data of surface tension (γ) versus the natural logarithm of the solute molar concentration; ln *C*, as shown in Fig. 7. The critical micelle concentration (CMC) indicated the value of concentration at which it becomes thermodynamically favorable for surfactant molecules to form aggregates (micelles) in order to minimize interaction of either their head groups or their tail groups with the solvent. Once the inhibitor concentration reaches a certain level (CMC), the water structure forces aggregation of the hydrophobic tail groups to form surfactant micelles.

Fig. 7 indicates that the synthesized EMB inhibitor is molecularly dispersed at low concentration, leading to a reduction in surface tension, until certain concentration is reached (CMC) the inhibitor molecules form micelles, which are in equilibrium with the free surfactant molecules.

3.4. Adsorption Isotherm Model

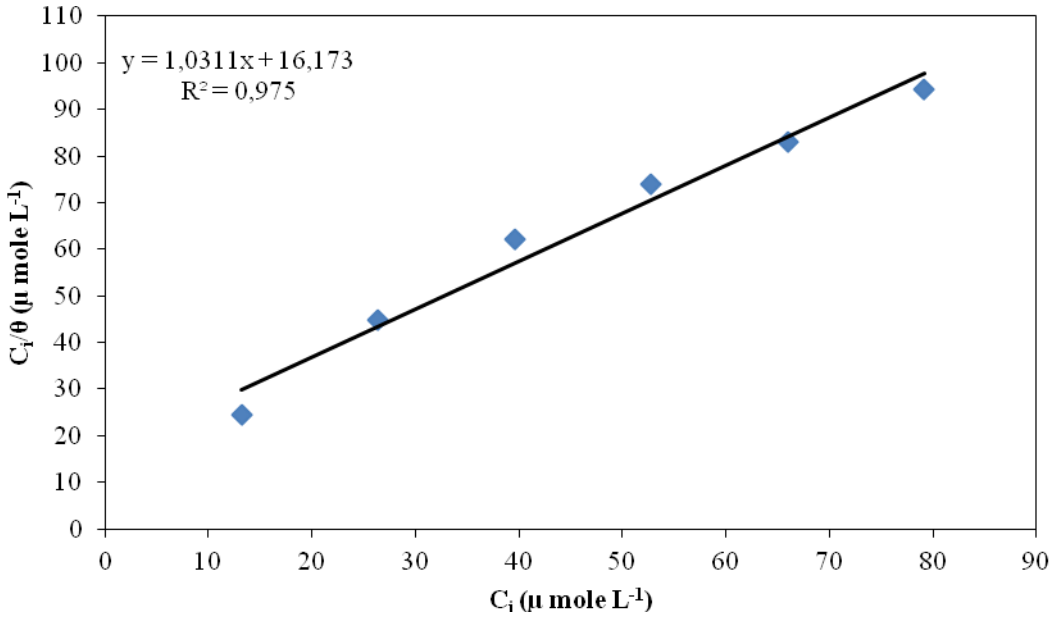

Figure 8. Langmuir adsorption isotherm model for the inhibitor on the carbon steel surface at 50 °C

Langmuir adsorption isotherm model was found to fit well with the obtained experimental data by plotting C_i / θ versus C_i [26-28].

$$C_i/\theta = 1/K_{ads} + C_i \quad (14)$$

where, C_i represents the molar concentration of the investigated EMB inhibitor and K_{ads} is the adsorption equilibrium constant. Fig. 8 shows a plotting of C_i / θ versus C_i straight line which have a slope of approximately equal unity, where a small deviation from unity is attributed to the interaction of adsorbed inhibitor molecules on heterogeneous carbon steel surface. Adsorption equilibrium constant K_{ads} is then calculated from the slope of Langmuir plots for the synthesized EMB inhibitor.

3.5. Standard Free Energy of Micellization Vs. Standard Free Energy of Adsorption

Standard free energy of micellization (ΔG^o_{mic}) for the synthesized EMB inhibitor was calculated using the obtained CMC values as per the following equation [29]:

$$\Delta G^o_{mic} = RT \ln CMC \quad (15)$$

while standard free energy of adsorption (ΔG^o_{ads}) was calculated as follows:

$$\Delta G^o_{ads} = - RT \ln K_{ads} \quad (16)$$

where K_{ads} is the adsorption equilibrium constant as calculated from Langmuir adsorption isotherm model.

Table 5. Standard free energy of micellization (ΔG^{o}_{mic}) and standard free energy of adsorption (ΔG^{o}_{ads}) as obtained from surface tension measurements and Langmuir adsorption isotherm model respectively at 50 ^{o}C

Standard Free Energy of Micellization, $-\Delta G^{o}_{mic}$ (kJ mol^{-1})	Standard Free Energy of Adsorption, $-\Delta G^{o}_{ads}$ (kJ mol^{-1})
19.7	29.6

The obtained values of standard free energy of micellization (ΔG^{o}_{mic}) and standard free energy of adsorption (ΔG^{o}_{ads}), as compared in Table (5), indicated that the synthesized inhibitor favors adsorption rather than micellization. This gives rise to formation of strong adsorption film on the metal surface which matches well with the results of electrochemical impedance and potentiodynamic polarization measurements.

3.6. Scanning electron microscopy (SEM)

(a)

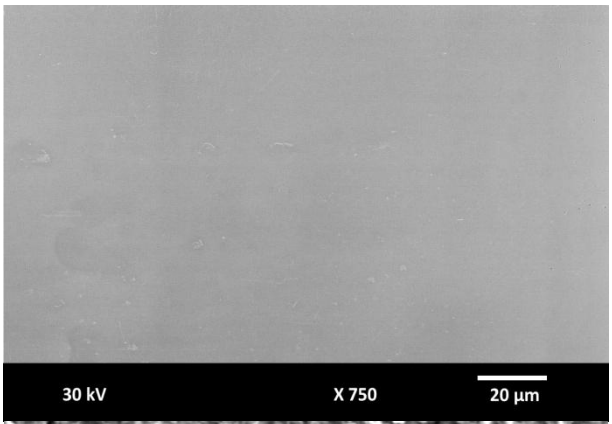

(b)

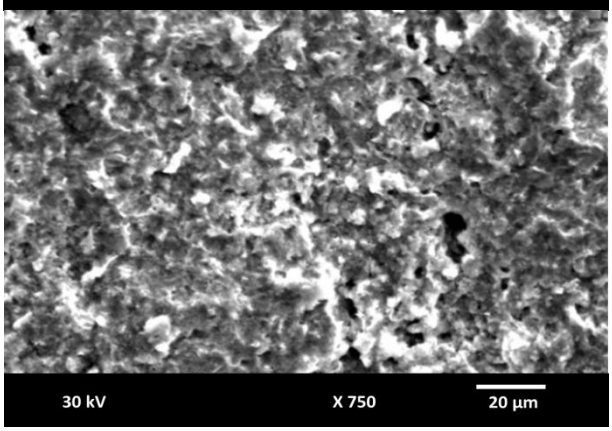

(c)

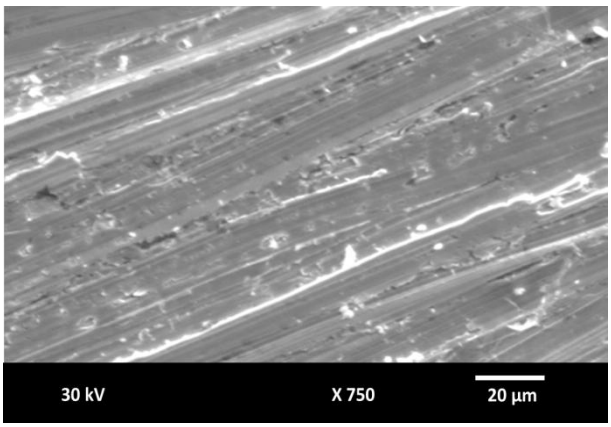

Figure 9. SEM images for the carbon steel surface: a) abraded sample, (b) after immersion in the oil wells produced water and (c) after immersion in the oil wells produced water in presence of 150 ppm of EMB inhibitor

Fig. 9a shows SEM image of abraded carbon steel surface. The micrograph shows a characteristic inclusion, which was probably an oxide inclusion [30]. Fig. 9b shows SEM of the surface of carbon steel specimen after immersion in produced water saturated with CO_2 at 50 ^oC for 30 days in absence of EMB inhibitor, while Fig. 9c shows SEM of another carbon steel surface after immersion in produced water saturated with CO_2 at 50 ^oC for the same time interval in presence of 150 ppm of the synthesized EMB inhibitor. Scanning electron micrographs indicates that carbon steel surface is quite less damaged in presence of 150 ppm of EMB inhibitor however was strongly damaged in absence of the inhibitor. This confirms the observed high inhibition efficiency of EMB inhibitor at this concentration.

3.7. Quantum chemical study results

Table 6. Quantum chemical parameters of the investigated inhibitor

Inhibitor	E_{HOMO}(eV)	E_{LUMO}(eV)	ΔE(eV)	μ(debye)	ΔN(eV)
I	-7.79	-0.273	7.51	1.614	-0.39

Quantum chemical studies have been successfully implemented to correlate the corrosion protection efficiency of organic inhibitor with its calculated molecular orbital (MO) energy level [31].

Some quantum chemical parameters which impact the electronic interaction between iron surface and inhibitor molecules are listed in Table (6), namely the energy of highest occupied molecular orbital (E_{HOMO}), energy of the lowest unoccupied molecular orbital (E_{LUMO}), the energy gap (ΔE), dipole moment (μ) and the number of transferred electrons (ΔN), while the optimized geometry structures of EMB inhibitor are shown in Fig. 10.

The inhibitive effect of EMB inhibitor can be attributed to its parallel adsorption at the metal surface. The parallel adsorption is attributed to the presence of one or more active centers for

adsorption. The results suggest a planar geometry of the inhibitor. The planer geometry is clear in Fig. 10, where approximately planar structure offers the largest contact area between the inhibitor molecules and the steel surface.

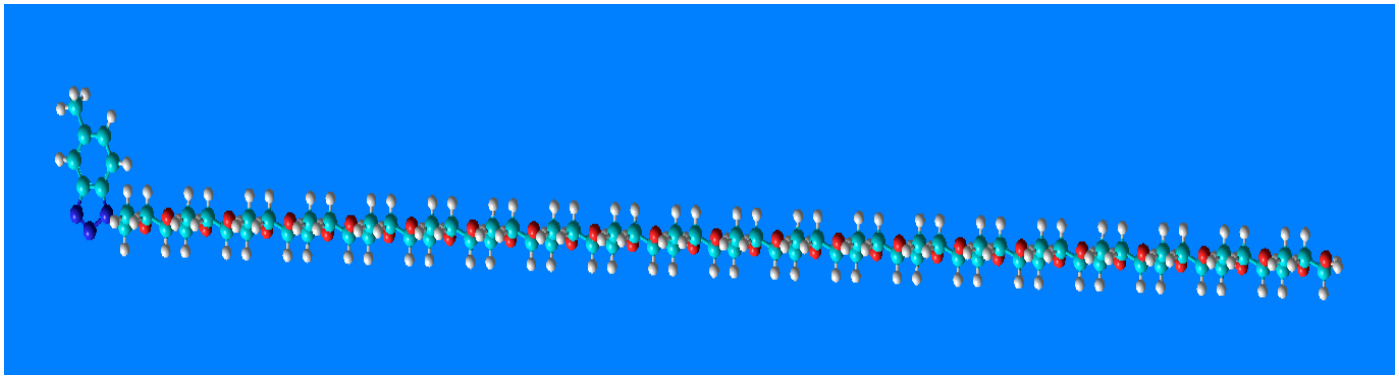

Figure 10. Equilibrium structure of the inhibitor

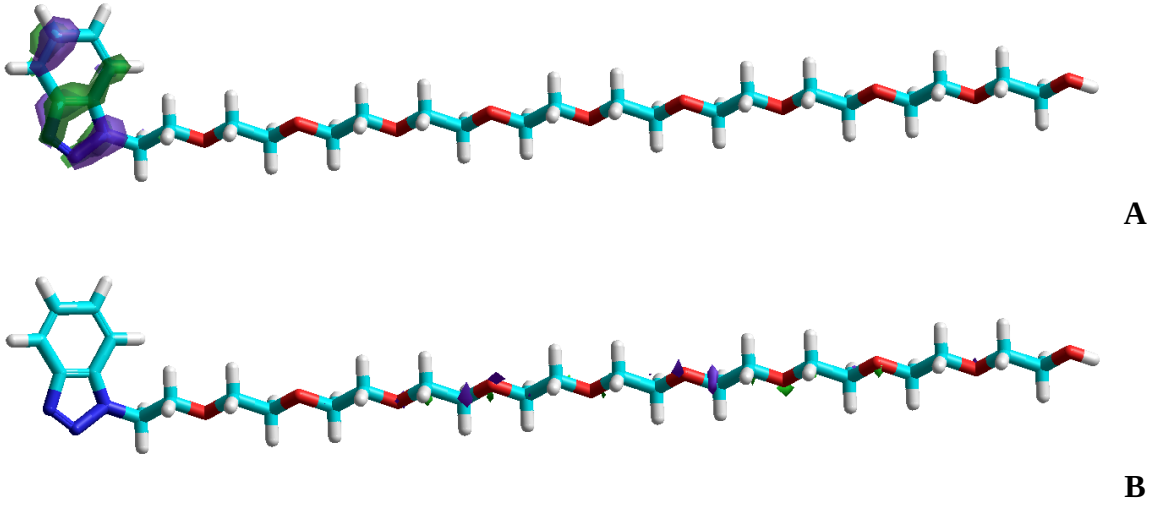

Figure 11. The frontier molecule orbital density distributions of Inhibitor (a) HOMO and (b) LUMO

Frontier orbital theory is useful in predicting adsorption centers of the inhibitor molecules responsible for the interaction with metal surface atoms [32,33]. Terms involving the frontier MO could provide dominative contribution, because of the inverse dependence of stabilization energy on orbital energy difference [34]. It has been reported in the literature that the higher the HOMO energy of the inhibitor, the greater the trend of offering electrons to unoccupied d orbital of the metal, and the higher the corrosion inhibition efficiency.

In addition, the lower the LUMO energy, the easier acceptance of electrons from metal surface, since the LUMO–HOMO energy gap decreased the efficiency of inhibitor improved [35]. The frontier molecule orbital density distributions for inhibitor are shown in Fig.11 (a,b). Quantum chemical

parameters listed in Table (6) reveal that this inhibitor has high HOMO and low LUMO with high energy gap. The number of transferred electrons (ΔN) was also calculated according to Eq. (17) [36,37]

$$\Delta N = \frac{X_{Fe} - X_{inh}}{2(\eta_{Fe} - \eta_{inh})} \quad (17)$$

where X_{Fe} and X_{inh} denote the absolute electronegativity of iron and EMB inhibitor molecule, respectively; η_{Fe} and η_{inh} denote the absolute hardness of iron and EMB inhibitor molecule, respectively. These quantities are related to electron affinity (A) and ionization potential

$$X = (I + A)/2 \quad , \quad \eta = (I - A)/2 \quad (18)$$

where I and A are related in turn to E_{HOMO} and E_{LUMO}

$$I = -E_{HOMO} \quad , \quad A = -E_{LUMO} \quad (19)$$

where values of X and η were calculated by using the values of I and A obtained from quantum chemical calculation. The theoretical values of X_{Fe} and η_{Fe} are 7 and 0 eV/mol, respectively [36]. The fraction of electrons transferred from inhibitor to the iron molecule (ΔN) was calculated. According to other reports [36,37], value of ΔN showed inhibition effect resulted from electrons donation.

The dipole moment (μ) is an index that can also be used for prediction of the direction of a corrosion inhibition process [38]. Low values of the dipole moment will favor the accumulation of inhibitor molecules on the metallic surface.

3.7.1. Molecular Electrostatic Potential

The molecular electrostatic potential (MEP) is related to the electronic density and is a very useful descriptor for determining sites for electrophilic attack and nucleophilic reactions as well as hydrogen-bonding interactions [39–41]. The electrostatic potential V(r) is also suited for analyzing adsorption processes based on the recognition of one molecule by another, since the two species first "see" each other [42,43]. As a physical property, V(r) can be determined experimentally by diffraction or by computational methods [44].

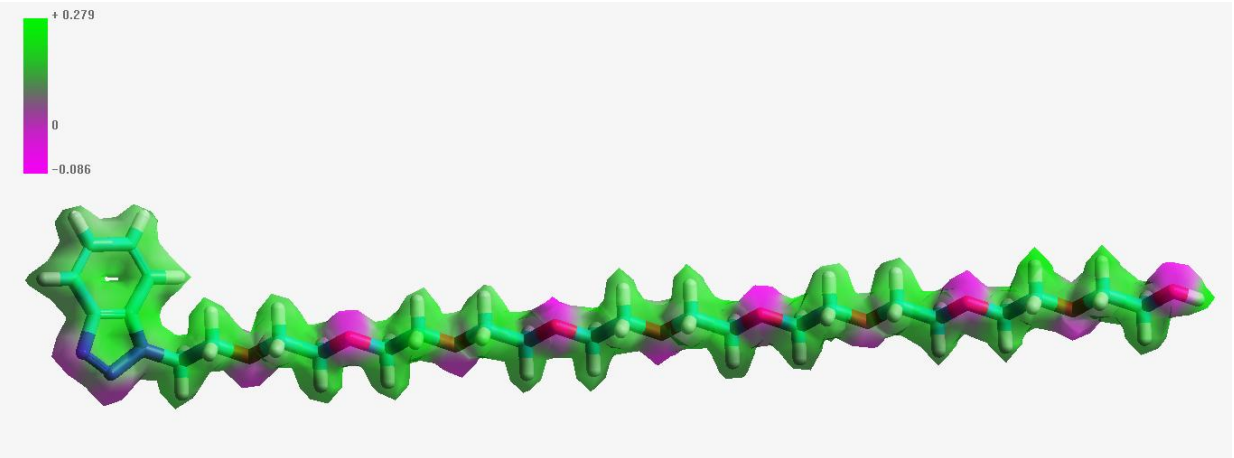

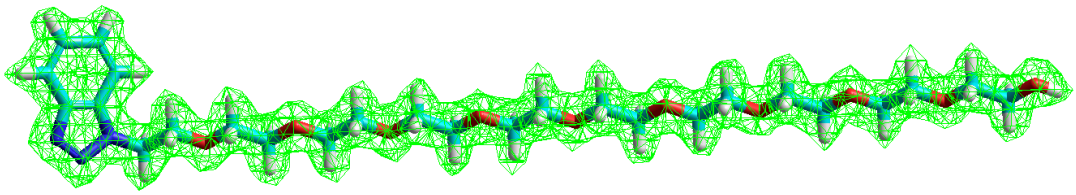

Figure 12. Molecular electrostatic potential map of the compound

Prediction of reactive sites for electrophilic and nucleophilic attack for EMB inhibitor molecule was carried out. The negative (red) regions of MEP indicate electrophilic reactivity while the positive (green) regions indicate nucleophilic reactivity as shown in Fig. 12 which illustrates a possible site on inhibitor molecule for electrophilic attack. The negative region is localized on the nitrogen atom with a maximum value of -0.46 a.u. and oxygen atom of ethylene oxide chain with value of -0.433 a.u.

However, a maximum positive region is localized on carbon atom, with a maximum value of 0.38 a.u. This result indicates a region where the inhibitor can interact intermolecular and bond covalently.

The Mulliken charge distribution of inhibitor is presented in Table (7).

Table 7. The charge density of some atoms in the inhibitor

No.	Atom	Charge
1	N	-0.460
2	N	-0.035
3	O	-0.403
4	O	-0.433
5	C	0.382

It could be observed that nitrogen atoms and oxygen of ethylene oxide had higher charge densities. The regions of highest electron density are generally the sites to which electrophiles attacked. Therefore N and O atoms were the active center, which had the strongest ability of bonding to the metal surface. On the other hand, HOMO (Fig. 11a) was mainly distributed on the area containing Nitrogen atom. Thus, the area containing nitrogen atom was probably the primary site of the bonding.

4. CONCLUSION

1. The investigated nonionic surfactant is effective inhibitor for corrosion of carbon steel in oil well produced water.

2. The adsorption of the inhibitor molecules obeyed the Langmuir adsorption isotherm.

3. The potentiodynamic polarization curves indicated that the inhibitor molecules inhibit both anodic metal dissolution and also cathodic oxygen reduction, so that the undertaken surfactant classified as mixed – type inhibitor.

4. The inhibition mechanism is attributed to the strong adsorption ability of the selected surfactant on carbon steel surface, forming a good protective layer, which isolates the surface from the aggressive environment.

5. The formation of a good protective film on carbon steel surface was confirmed using SEM and EDX techniques.

6. The data obtained from the experimental techniques are confirmed by theoretical data obtained from quantum chemical calculations.

ACKNOWLEDGEMENTS
The authors would like to express their appreciation for Egyptian Petroleum Research Institute (EPRI) for the financial support of this work.

References

1. D.A. Lopez, S.N. Simison, S.R. de Sanchez, *Electrochim. Acta* 48 (2003) 845.
2. P. Altoe, G. Pimenta, C. F. Moulin, S. L. diaz, O. R. Mattos, *Electrochem. Acta* 41(1996) 1165 – 1172.
3. M. W. S. Jawich, G. A. Oweimreen, S. A. Ali ; *Corros. Sci.* 65 (2012) 104–112
4. M. A. Migahed, J. Banaś., U. Lelek-Borkowska, K. Kowalski, Corrosion inhibition of carbon steel in aqueous media at elevated temperature and under high pressure of CO_2, In proceedings of Eurocor 2006, Maastrichit,Netherlands. P.
5. G. A. Zhang, Y. F. Cheng, *Corros. Sci.* 51 (2009) 87-94.
6. G. Schmitt, Corrosion, NACE, vol. 1, p. 1 (1985).
7. W. Schulz, M. Nofz, M. Feigl , I. Dörfel, R. Saliwan Neumann, A. Kranzmann; *Corros. Sci.* 68 (2013) 44–50
8. J.H.Clint; Surfactant Aggregation, Blackie, Glasgow and London,Chapman & Hall, New York, 1992.
9. A. J. McMahon.; *Coll. Surf.* 59 (1991) 187.
10. M.M., Osman, A.M.A.Omar, A.M Al.sabagh.; *Mat. Chem. and Phys.* 50 (1997) 271.
11. F.Hanna, G.M.Sherbini, Y.Brakat; *Brit. Corros. J.*, 24 (1989) 269.
12. M.M .Osman., M.N.Shalaby; *Mat. Chem. and Phys.* 77 (2002) 261.
13. A.M.Alsabagh; M.A.Migahed , Hayam. S. Awad S.; *Corros. Sci.* 48 (2006) 813.
14. M.A .Migahed, M.Abd-El-Raouf, A.M. Al-Sabagh, H.M.Abd-El-Bary; *Electrochim. Acta* , 50 (2005) 4683.
15. M.A .Migahed., H.M.Mohamed, A.M.Al-Sabagh; *Mat. Chem. and Phys.* 80 (2003) 169.
16. M. Behpour, N. Mohammadi; *Corros. Sci.* 65 (2012) 331–339
17. W.Hreczuch,A. Kozlek; Tens. *Surf. Det.* 38 (2) (1996) 621.
18. W.Hrec Zuch andA. Kozlek.; *Tens. Surf. Det.* 38 (1996) 621.
19. Van Os, N.M., Non-Ionic surfactant "Organic chemistry", Surfactant science series, volume 72, Marcel Dekker, New York, (1998).
20. R.F Lang ., Diaz.P.D and Jocobs.D.; *J. Surf. Det.* , 7(1999) 503.

21. K.F. Khaled, *Electrochim. Acta* , 48 (17) (2003) 2493.
22. Q.B.Zhang; Y.X Hua.; *Electrochim. Acta* , 54 (2009) 1881.
23. A. P.; Yadav,A. Nishikata; Tsuru T.; *Corros. Sci.*, 46(2004)169.
24. K.F.Khaled; *Appl. Surf. Sci.* 252 (2006) 4120.
25. M.A. Migahed, M.A. Hegazy, A.M. Al-Sabagh; *Corros. Sci.*, 61 (2012) 10 -18
26. G.Saha; N. Kurmaih; *Corros.* 42 (1986) 9.
27. I.Sekine; Y.Hirakawa; *Corros.* 42 (1986) 272.
28. I.Sekine; T.Shimode; Yuasa M.; Takaoka K.; *Ind. Eng. Chem. Res.*, 29 (1990)1460.
29. J.Rosen Milton; Surfactants and Interfacial Phenomena, Third Edition, John Wiley & Sons Inc. (2004)
30. ASTM E 45-87, vol. 11, ASTM, Philadelphia, PA, (1980) 125.
31. M. J., Bahrami , S.M. A. ,Hosseini and P.Pilvar (2010) *Corros. Sci.* 52 (2793)
32. J. Fang, J. Li, *J. Mol. Struct.* (THEOCHEM) 593 (2002) 179.
33. G. Bereket, E. Hur, C. Ogretir, *J. Mol. Struct.* (THEOCHEM) 578 (2002) 79.
34. A.Y. Musa, A.A.H. Kadhum, A.B. Mohamad, M.S. Takriff, A.R. Daud, S.K. Kamarudin, *Corros. Sci.*, 52 (2010) 526.
35. K.F. Khaled, *Appl. Surf. Sci.* 255 (2008) 1811.
36. H. Ju, Z. Kai, Y. Li, *Corros. Sci.* 50 (2008) 865.
37. I. Lukovits, E. Kalman, F. Zucchi, Corrosion (NACE) 57 (2001) 3.
38. C.Hansch,; A.Leo, Substituentz for Correlation Analysis in Chemistry and Biology; Wiley: New York, NY, USA, 1979.
39. E.Scrocco, , & J. Tomasi, (1979). *Adv. Quant. Chem.*, 11, 115.
40. F. J.Luque, , J. M .Lopez, & Orozco, M. (2000). *Theor. Chem. Accounts*, 103, 343.
41. N.Okulik, & A. H. Jubert, (2005). *Internet Electron. J. Mol. Des.*, 4, 17.
42. P.Politzer, , P. R.Laurence, , & K.Jayasuriya, (1985). *Environ. Health Perspect.* [Special issue], 61, 191.
43. E.Scrocco, , & J.Tomasi, (1973). Topics in Current Chemistry, Springer: Berlin.
44. P.Politzer, , & D. G. Truhlar, (1981). Chemical Applications of Atomic and Molecular Electrostatic Potentials, Plenum: New York.